### Title

Calcium-responsive contrast agents for functional magnetic resonance imaging




### Journal

Chemical Physics Reviews, 2(2)

### ISSN

2688-4070



### Authors

Miller, Austin DC
Ozbakir, Harun F
Mukherjee, Arnab



### Publication Date

2021-06-01

### DOI

10.1063/5.0041394

Peer reviewed

Chemical Physics Reviews REVIEW scitation.org/journal/cpr

# Calcium-responsive contrast agents for functional magnetic resonance imaging

Cite as: Chem. Phys. Rev. **2**, 021301 (2021); doi: 10.1063/5.0041394
Submitted: 22 December 2020 · Accepted: 15 March 2021 ·
Published Online: 20 April 2021



Austin D. C. Miller,[1] Harun F. Ozbakir,[2] and Arnab Mukherjee[1,2,3,4,5,a)]

## AFFILIATIONS

[1]Biomolecular Science and Engineering, University of California, Santa Barbara, California 93106, USA
[2]Department of Chemical Engineering, University of California, Santa Barbara, California 93106, USA
[3]Department of Chemistry, University of California, Santa Barbara, California 93106, USA
[4]Neuroscience Research Institute, University of California, Santa Barbara, California 93106, USA
[5]Center for Bioengineering, University of California, Santa Barbara, California 93106, USA

[a)]**Author to whom correspondence should be addressed:** arnabm@ucsb.edu. **Tel.:** (805) 893-5137

## ABSTRACT

Calcium ions represent one of the key second messengers accompanying neural activity and synaptic signaling. Accordingly, dynamic imaging of calcium fluctuations in living organisms represents a cornerstone technology for discovering neural mechanisms that underlie memory, determine behavior, and modulate emotional states as well as how these mechanisms are perturbed by neurological disease and brain injury. While optical technologies are well established for high resolution imaging of calcium dynamics, physical limits on light penetration hinder their application for whole-brain imaging in intact vertebrates. Unlike optics, magnetic resonance imaging (MRI) enables noninvasive large-scale imaging across vertebrates of all sizes. This has motivated the development of several sensors that leverage innovative physicochemical mechanisms to sensitize MRI contrast to intracellular and extracellular changes in calcium. Here, we review the current state-of-the-art in MRI-based calcium sensors, focusing on fundamental aspects of sensor performance, *in vivo* applications, and challenges related to sensitivity. We also highlight how innovations at the intersection of reporter gene technology and gene delivery open potential opportunities for mapping calcium activity in genetically targeted cells, complementing the benefits of small molecule probes and nanoparticle sensors.



## TABLE OF CONTENTS



## I. INTRODUCTION

Understanding the large-scale dynamics of neural signaling holds one of the keys to discovering how the brain encodes experience, modifies behavior, recovers from injury, and degenerates. The most widely used approach for imaging neural activity relies on fluorescent dyes and genetic indicators,[1–3] which change their spectral properties in response to an increase in cellular calcium that coincides with neural activation.[4,5] When combined with advanced microscopy techniques such as 2- and 3-photon imaging, calcium-sensitive indicators can detect activity in single neurons up to depths of 1 mm inside the vertebrate brain, although the imaging volume (~1 mm$^3$) covers only a fraction of the whole brain (~0.2% of the total brain volume in mice).[6–14] Alternatively, calcium signals can be detected in deeper regions by implanting fiber optic cannulae and specialized rod-shaped lenses, but these methods are invasive, and the imaging field covers a limited area (~0.2–0.5 mm diameter).[15–17] Thus, despite prolific advances in calcium dyes, genetic reporters, and optical technology, the limitation of light scattering hinders optical methods from achieving deep-tissue, brain-wide visualization of calcium signaling dynamics in vertebrates. Given that simultaneous imaging of multiple regions throughout the brain is necessary to decode the neural

representation of behaviors ranging from cognitive function to sensorimotor activity, as well as the large-scale effects of neuromodulation and neurological disorders, the lack of whole-brain access represents a significant limitation of optical calcium sensors. In contrast to optical methods, magnetic resonance imaging (MRI) can noninvasively access large tissue volumes located at any arbitrary depth, achieving fairly high spatial (200–400 $\mu$m) and temporal resolution (seconds) in experimental vertebrates of all sizes.[18–21] As an added benefit, the MRI field of view includes surrounding tissues and thus provides anatomical context to images. These attributes make MRI very attractive for large-scale calcium imaging, prompting the development of several MRI probes that produce contrast in response to calcium.[22–45] At the same time, curbs on MRI sensitivity and the modest signal changes obtained with most contrast agents (response magnitude is often on the order of its standard deviation) impose a unique set of challenges for applying MRI sensors to image calcium dynamics *in vivo*. In this review, we focus on the main classes of calcium-responsive MRI probes currently available and describe the chemico-physical mechanisms by which they detect and respond to calcium. We discuss key determinants of sensor performance, including response amplitude, calcium affinity, physiological range of calcium fluctuations, and delivery limitations imposed by various probe architectures. We also highlight pioneering examples of *in vivo* neural activity imaging using calcium-responsive MRI sensors. We close by identifying avenues where parallel innovations in MRI technology, molecular biology, protein engineering, and gene delivery promise to establish new capabilities for whole-brain calcium imaging, including heightened sensitivity and genetic targetability.

## II. SMALL MOLECULE $T_1$ SENSORS FOR DETECTING INTRACELLULAR CALCIUM FLUCTUATIONS

The paradigmatic sensor architecture for detecting calcium ions with MRI comprises organic complexes of $Gd^{3+}$ conjugated to a calcium chelating molecule via flexible linkers [Fig. 1(a)].[22,23,25,29,39] When calcium concentration is low (e.g., 50–100 nM in the resting state of neurons) the negatively charged carboxylate or phosphonate groups of the calcium chelator coordinate the paramagnetic $Gd^{3+}$ ions, blocking bulk water molecules from interacting with the metal. Calcium chelation causes the carboxylate or phosphonate arms to swing away from the paramagnetic center, freeing up the $Gd^{3+}$ ions to interact directly with water [Fig. 1(a)].[23,29] This conformational switch leads to stronger water-metal interactions in the calcium-bound state relative to the unbound sensor, which can be visualized in MRI due to an increase in the spin-lattice relaxation rate ($T_1$ relaxation, Appendix) of water protons. Calcium sensors based on this principle have been found to elicit maximum relaxivity changes (relaxation rate per mM of the sensor) ranging from 1.4- to 2.2-fold between calcium-free and saturated conditions (Table I).[22,36,39,42] The prototypical sensor in this class (introduced by Meade and colleagues[22]), comprising two macrocyclic $Gd^{3+}$ complexes bridged by a BAPTA-based calcium chelator, is activated by the intracellular range of calcium concentrations (0.1–10 $\mu$M) owing to its high calcium affinity ($K_d \sim 1\ \mu$M) and selectivity over divalent metal ions such as $Mg^{2+}$. However, the four units of negative charge carried by BAPTA make it challenging to deliver the probe inside cells at concentrations necessary to image calcium fluctuations. To solve this problem, Meade and colleagues neutralized the negative charge of the BAPTA carboxylates by adding ester groups.[36] Upon entering a cell, the ester groups are removed by cytoplasmic esterases with a pseudo first

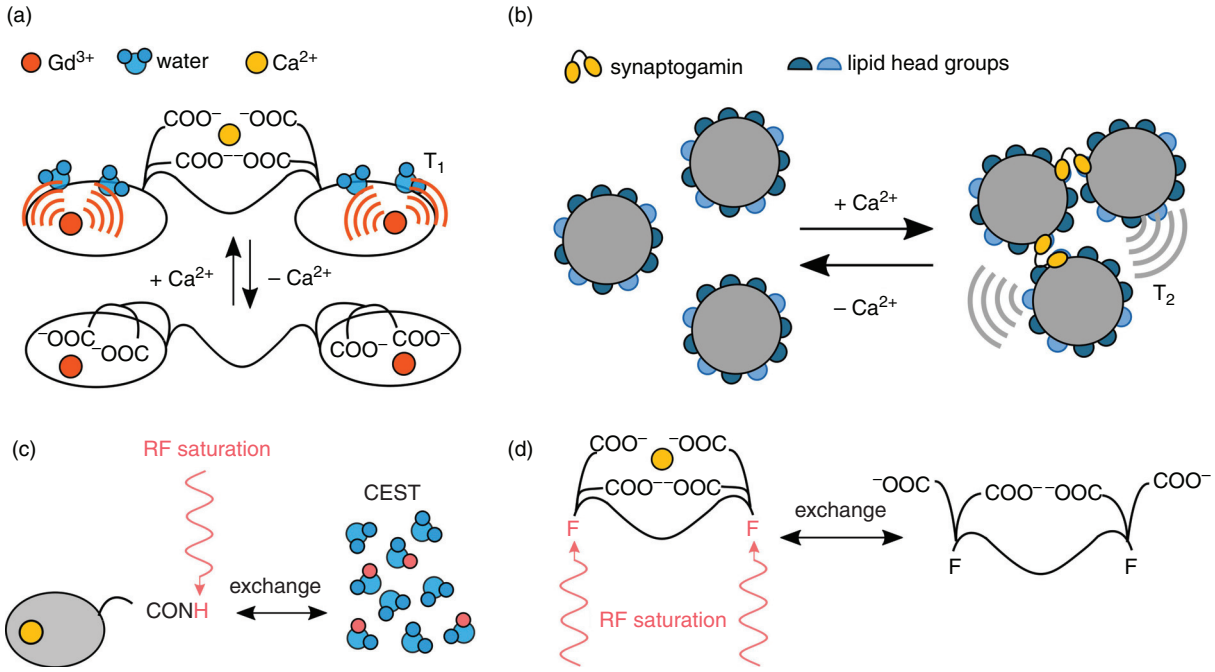


**FIG. 1. Key mechanisms for designing calcium-responsive MRI sensors**. (a) $T_1$ sensors based on calcium-controlled water access to a paramagnetic metal center. (b) Superparamagnetic iron oxide nanoparticle sensors based on calcium-induced clustering and changes in $T_2$ relaxation. (c) Basic principle of chemical exchange saturation transfer (CEST). (d) Schematic of calcium sensor based on integration of $^{19}F$ MRI and CEST.

**TABLE I.** Key performance characteristics of common $T_1$-based calcium indicators. Here, $r_{1,on}$ and $r_{1,off}$ refer to $T_1$ relaxivities in the presence and absence of calcium respectively. For sensors that have not been tested *in vivo*, we computed a theoretical upper bound for percent change in $T_1$ weighted MRI signal intensity $(\Delta SI/SI)_{max}$ as described in Appendix.

| $T_1$ agents | $r_{1,on}$ $mM^{-1}$ $s^{-1}$ | $r_{1,off}$ $mM^{-1}$ $s^{-1}$ | $K_d$ $\mu M$ | $(\Delta SI/SI)_{max}$ predicted | $\Delta SI/SI$ *in vivo* | MRI field strength (T) |
|---|---|---|---|---|---|---|
| DOPTA-Gd(III)[22] | 5.76 | 3.26 | 0.96 | 3.2 % | | 11.75 |
| DOPTA-Ethyl-Gd(III)[36] | 12.6 | 10.6 | 16.6 | 1.2 % | | 1.41 |
| IR783 DOPTA-Gd(III)[42] | 9.6 | 4.4 | 3.6 | 5.4 % | | 7 |
| ManICS1[39] | 5.1 | 3.6 | 18 | | 5.8 % upon stimulation with $K^+$ ions | 7 |
| APTRA-based Gd(III) sensor for extracellular calcium[27] | 6.9 | 3.5 | 11 | 6.5 % | | 9.4 |
| EGTA-derived Gd(III) sensor for extracellular calcium[25,32] | 3.64 | 2.42 | 45.4 | | 2%–4% in stroke model | 11.75 |
| Ultrasmall rigid particle with EGTA-Gd(III) extracellular sensor[35] | 7.03 | 3.6 | 1900 | | 30% in the renal pelvis subsequent to $CaCl_2$ injection | 7 |

order rate constant of 0.061 $h^{-1}$ ($t_{1/2} = 11.4$ h), thereby freeing the sensor to respond to calcium. Using this approach, cells could be stably filled with high concentrations of the sensor (> 1 mM after 4 h incubation with 125 $\mu$M sensor) and exhibited < 10% washout over a 24-h period. In another innovative approach from the same group, cellular uptake was further improved by conjugating a near infrared dye (IR-783) without modifying the sensor's negative charge, instead relying on the ability of IR-783 to reliably deliver small molecules to cells via drug transporters known as organic anion transporter polypeptides (Oatp).[42] The improved uptake synergized with the sensor's substantial relaxivity change (2.2-fold) and strong calcium affinity ($EC_{50} = 3.6$ $\mu$M), enabling the detection of ionophore-mediated calcium entry in a neuronal cell line (HT-22). The first *in vivo* proof-of-concept was led by the Jasanoff group, which developed a probe consisting of an $Mn^{3+}$ complex conjugated to a BAPTA chelator modified with ester groups to promote cellular uptake and retention.[39] Following bolus injection of this probe over a ~36 $\mu$L brain volume located 0.5 cm deep from the skull, the authors could track increase in $T_1$ weighted signal intensity at 0.2 Hz temporal resolution during neuronal depolarization induced by infusing $K^+$ ions in the same brain region where the sensor had been injected [Fig. 2(a)].

## III. SMALL MOLECULE $T_1$ PROBES FOR IMAGING CALCIUM CHANGES IN THE EXTRACELLULAR MILIEU

The extracellular space in brain contains around 1.2 mM calcium that can drop by 30% during intense electrical activity and by as much as 90% in pathological states characterized by seizures and ischemia.[46,47] Thus, there is considerable interest in detecting extracellular calcium for applications in basic biology as well as molecular diagnostics. The low $\mu$M affinity of BAPTA-based calcium indicators (Table I), while useful for sensitizing MRI response across the full two log range of intracellular calcium changes, limits their utility for imaging the substantially smaller amplitude of calcium variations occurring in the extracellular space. As a result, initial efforts to image variations in extracellular calcium involved conjugating paramagnetic $Gd^{3+}$ complexes to weaker calcium chelators such as APTRA and bisphosphonates.[27,29] Alternatively, substituting one of the two carboxylate pairs

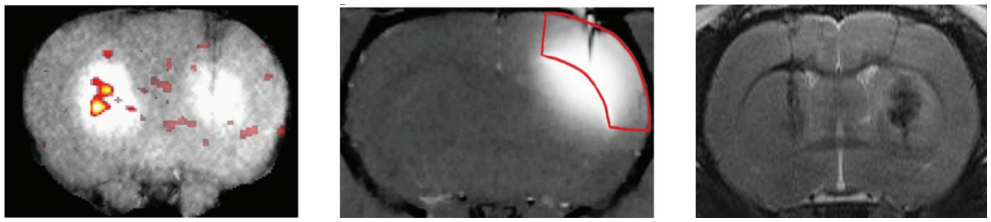

(a) (b) (c)

**FIG. 2. Molecular MRI using calcium-responsive sensors**. (a) Imaging neural activity induced by $K^+$ infusion, using a $T_1$-based intracellular calcium sensor, ManICS1 acutely loaded in the left hemisphere. (b) Continuous infusion from an osmotic pump enables small molecule calcium probes to be maintained at steady concentrations over a relatively large area of the brain. (c) Application of alginate-coated iron oxide nanoparticles to detect quinolic acid induced brain injury based on an increase in the number of hypointense, i.e., $T_2$ weighted, voxels in right hemisphere relative to the sham-injected left hemisphere. Images in (a) and (b) are reproduced from A. Barandov, B. B. Bartelle, C. G. Williamson, E. S. Loucks, S. J. Lippard, and A. Jasanoff, Nat. Commun. **10**(1), 897 (2019)[39] and T. Savić, G. Gambino, V. S. Bokharaie, H. R. Noori, N. K. Logothetis, and G. Angelovski, Proc. Nat. Acad. Sci. **116**(41), 20666–20671 (2019),[41] respectively, via a Creative Commons Attribution 4.0 International License: http://creativecommons.org/licenses/by/4.0/. Image in (c) is reproduced with permission from A. Bar-Shir, L. Avram, S. Yariv, -Shoushan, D. Anaby, S. Cohen, N. Segev-Amzaleg, D. Frenkel, O. Sadan, D. Offen, and Y. Cohen, NMR Biomedicine **27**(7), 774–783 (2014).[45] Original figures have not been modified except for cropping to fit within the page margins.

in EGTA with amide functions was found to lower calcium affinity without affecting selectivity over divalent ions such as $Mg^{2+}$.[25,32] The resulting EGTA-based probe operates by a similar mechanism as the previous intracellular sensors, but on account of its higher $K_d$ (45.4 $\mu$M, Table I) can be used externally, as demonstrated by MRI detection of a 1.2- to 0.8-mM step change in extracellular calcium in 3D fibroblast cultures.[32] However, a critical challenge for detecting calcium fluctuations across such narrow millimolar-scale intervals is that high concentrations of the probe are needed to obtain reliable changes in MRI signal. For instance, in the aforementioned example, 1.2-mM probe concentration was required to elicit 2.4% average change in $T_1$ relaxation rate. Such concentrations may be difficult to achieve *in vivo* and can potentially perturb cell physiology by buffering free calcium. To this end, Angelowski *et al.* reported a remarkable 64%–67% drop in cytoplasmic calcium levels of primary astrocytes within 5 min of incubating the cells with the above EGTA-derived sensor, although no acute toxicity was observed for 4 h following exposure.[32] Another limitation of small molecule probes that do not enter cells relates to their rapid diffusion ($D \sim 0.2\ \mu m^2/ms$) and clearance ($t_{1/2} = 1.4$–$2.9$ h) from the extracellular space.[48] As a result, variations in local probe concentration due to pharmacokinetics and diffusion may limit the accuracy with which the $T_1$ change in a given voxel can be assigned to an authentic fluctuation in calcium levels. Despite these challenges, the aforementioned EGTA-based calcium sensor was recently applied in an exciting *in vivo* application to monitor the time course of calcium changes induced by transient middle cerebral artery occlusion in rats, a well-established model of stroke.[41] Here, the authors continuously infused the sensor from an osmotic pump, which enabled dynamic imaging (0.05-Hz frame rate) of extracellular calcium as its levels first dropped during the ischemic phase (manifested as 2%–4% decrease in $T_1$ weighted intensity) and then recovered once blood flow was re-established by removing the arterial occlusion. By relying on continuous osmotic infusion, the authors were also able to compensate for potential changes in probe concentration and maintain stable sensor levels over a reasonably large portion of the rat brain (~20%) [Fig. 2(b)]. Another approach for maintaining steady state sensor concentrations involves slowing probe diffusion and washout by attaching the small molecule sensor to macromolecular scaffolds such as dendrimers, liposomes, or ultrasmall (<5.5 nm diameter) rigid particles of polysiloxane.[34,35,44,49] Of these, the last architecture has been assessed in preliminary *in vivo* experiments by visualizing calcium increase in the fluid-filled renal pelvis of mice following intravenous co-injection of the contrast agent and $CaCl_2$; however, signal changes in the renal cortex were not statistically significant.[35] In addition to bestowing favorable pharmacokinetic properties, macromolecular scaffolds tend to improve relaxivities of small molecule $T_1$ sensors at low to intermediate magnetic fields due to a slowing down of the sensor's rotational correlation time, which makes these probes particularly useful for applications in 0.5–1.5 Tesla bench-scale MRI scanners.[44,49] A compiled list of major $T_1$-based calcium sensors together with their MRI properties is enumerated in Table I.

## IV. $T_2$ SENSORS FOR CALCIUM BASED ON SUPERPARAMAGNETIC IRON OXIDE NANOPARTICLES

With the goal of generating larger changes in MRI signal in response to the modest amplitude of extracellular calcium variations, superparamagnetic iron oxide nanoparticles (20–100 nm diameter) have been engineered to reversibly cluster based on the occurrence of calcium ions in the milieu.[24,38,45] Magnetic nanoparticles generate MRI contrast by accelerating spin-spin relaxation ($T_2$ relaxation, Appendix) of water molecules due to a loss of phase coherence among nuclear spins of water protons as they diffuse through magnetic gradients created in the neighborhood of the nanoparticle. The $T_2$ relaxivities of superparamagnetic iron oxide nanoparticles are at least 10-fold larger than the $T_1$ relaxivities of most small molecule probes (Tables I and II), thereby enabling imaging with enhanced sensitivity. Furthermore, $T_2$ effects are sensitive to the aggregation state of nanoparticles, which constitutes the primary mechanism of sensors built on this principle [Fig. 1(b)].[50] The first-generation of calcium nanosensors, pioneered by the Jasanoff group, employed two types of streptavidin-coated iron oxide nanoparticles—one conjugated to biotinylated calmodulin and the other to short calmodulin-binding peptides (CBP) such as RS20 and M13.[24] Calmodulin–CBP pairs are widely exploited in the design of fluorescent calcium indicators due to their reversible and calcium-dependent binding properties. The resulting calmodulin and CBP-functionalized nanoparticles were found to cluster when mixed in the presence of calcium, producing a fivefold decrease in $T_2$ relaxivity—much larger than $T_1$ changes typically observed with small molecule sensors (Tables I and II). An added

**TABLE II.** Key performance characteristics of $T_2$-based calcium indicators. Here, $r_{2,on}$ and $r_{2,off}$ refer to $T_2$ relaxivities (per Fe) in the presence and absence of calcium, respectively.

| $T_2$ agents | $r_{2,on}$ $mM^{-1}\ s^{-1}$ | $r_{2,off}$ $mM^{-1}\ s^{-1}$ | $K_d$ $\mu$M | $\Delta SI/SI$ *in vivo* | MRI field strength (T) |
|---|---|---|---|---|---|
| M13/CBP conjugated iron oxide nanoparticles[24] | 45[a] | 220 | 0.8–10 | | 4.7 |
| Alginate coated iron oxide nanoparticles[45] | not reported | not reported | not reported | ~2-fold increase in number of (hypointense) voxels following quinolic acid injury | 7 |
| Synaptogamin-based clustering of lipid coated iron oxide nanoparticles[38] | 261[a] | 151 | 430 | 10%–18% with various stimuli: $K^+$ infusion, glutamate, electrical | 7 |

[a]Notably, the relaxivity changes induced by calcium trend in opposite directions for the M13/CBP and synaptogamin nanoparticles, which likely relates to differences in diameters of the two particles. In particular, the larger size of M13/CBP clusters places them in the so-called static dephasing regime, where diffusion ceases to impart a significant effect on spin-spin relaxation, resulting in a decrease in $T_2$ relaxivity upon calcium-induced aggregation.

benefit of leveraging proteins as sensing elements is that molecular biology techniques can be applied to tune calcium binding properties. For instance, calcium affinity of the aforementioned nanoparticles could be varied by a full order of magnitude (Table II) simply by introducing point mutations. Alternatively, nanoparticle-based sensors have been developed by coating iron oxide particles with alginate, which promotes aggregation in the presence of calcium.[45] While alginate-based nanosensors have been applied to image extracellular calcium fluctuations induced by chemically injuring the brain with quinolic acid [Fig. 2(c)], a practical challenge is posed by the tendency of these particles to precipitate at high calcium concentrations (>0.5 mM). More recently, the Jasanoff group introduced a new class of calcium sensors based on the calcium-binding protein synaptogamin, which binds anionic lipids such as phosphatidylserine in the presence of calcium.[38] By coating iron oxide nanoparticles with specific anionic lipid compositions and mixing with bacterially purified synaptogamin, it was possible to control cluster assembly is response to calcium [Fig. 1(b)]. Although the resulting sensors produced a lower (1.72-fold) change in $T_2$ relaxivity compared to the calmodulin–CBP version, the larger $EC_{50}$ (430 $\mu$M) made them ideal for detecting extracellular calcium fluctuations. Furthermore, the synaptogamin-based nanosensors were found to assemble and dissociate with significantly faster kinetics (seconds range) than previous designs (tens of minutes).[24,38] Accordingly, these sensors enabled dynamic monitoring of extracellular calcium fluctuations, at frame rates ranging from 0.08 to 0.25 Hz in response to chemical stimulation with glutamate, infusion of $K^+$ ions, as well as electrical stimulation, thus providing one of the most comprehensive demonstrations to date of *in vivo* calcium imaging with MRI. A complete list of $T_2$-based calcium sensors together with their MRI properties is enumerated in Table II.

## V. CALCIUM IMAGING BASED ON ALTERNATIVE MECHANISMS: CEST AND $^{19}$F MRI

Aside from modulating $T_1$ and $T_2$ relaxation rates of bulk water, MRI contrast agents have also been developed based on a mechanism known as chemical exchange saturation transfer (CEST).[51] Here, the contrast agent harbors protons that resonate at a frequency shifted from that of water and that can exchange with bulk water protons. These exchangeable protons can be selectively saturated by irradiating at their resonance peak. As the saturated protons exchange with bulk water, they serve to attenuate the magnetization of water protons, reducing the net MRI signal intensity [Fig. 1(c)]. The CEST effect is activated only upon the application of an on-resonance radio frequency pulse. Thus, it can be used to acquire difference images with minimal background from unlabeled regions of tissue. The first calcium sensor to operate via CEST comprised a macrocyclic complex of $Yb^{3+}$ with frequency-shifted (~13 ppm) protons provided by carboxamide groups that produced a 60% reduction in water signal during CEST.[30] Calcium binding to this complex was found to slow down proton exchange nearly 10-fold resulting in diminished CEST effect. Unfortunately, the $Yb^{3+}$-based sensor was also sensitive to $Mg^{2+}$ ions and required very high concentrations (tens of mM) of the probe to generate detectable CEST effects. More recently, a CEST sensor for calcium was developed based on a $Co^{2+}$ complex harboring exchangeable carboxamide protons together with a crown ether for chelating calcium.[40] Here, calcium binding shifted the resonance frequency of the carboxamide protons from 77 to 80 ppm. Although the crown ether architecture improved selectivity for calcium over $Mg^{2+}$, the overall signal remained weak, requiring millimolar levels of probe to generate a 6.5% CEST effect.

An alternative to detecting MRI signals arising from water protons involves direct imaging of $^{19}$F nuclei using fluorinated contrast agents. As $^{19}$F concentration is negligible in soft tissues, fluorinated agents enable zero-background MRI and quantitative detection. One approach for coupling $^{19}$F signals to calcium fluctuations involves bridging an AAZTA-based $Dy^{3+}$ complex to perfluorinated t-butyl ether (that serves as the $^{19}$F agent) via a calcium chelator derived from EGTA. Upon calcium binding, the $^{19}$F nuclei approach the $Dy^{3+}$ ion, which results in reduction of the $^{19}$F signal due to paramagnetic relaxation enhancement.[43] Another interesting mechanism for developing $^{19}$F-based calcium probes involves the use of fluorinated peptide amphiphiles that self-assemble into nanoribbons in the presence of calcium, resulting in a reduction in $^{19}$F MRI intensity in proportion to calcium concentrations in the 2–6 mM range.[37] A particularly innovative approach for imaging calcium was introduced by Bar-Shir and colleagues, who combined the benefits of $^{19}$F MRI with CEST [Fig. 1(d)].[31] Here, the contrast agent comprised a fluorinated derivative of BAPTA known as 5F-BAPTA. Upon calcium binding, the $^{19}$F resonance in 5F-BAPTA shifts by 6 ppm relative to 5F-BAPTA in the calcium-free state, enabling selective saturation of $^{19}$F spins in the bound state. As the saturated $^{19}$F nuclei exchange with the pool of $^{19}$F spins in calcium-free 5F-BAPTA, they result in ~11% reduction in $^{19}$F MRI signals recorded from the unbound 5F-BAPTA pool. Importantly, this approach enables detection of much lower calcium concentrations (~0.5 $\mu$M) taking advantage of the fact that the $^{19}$F spins in the calcium-bound complex need to exchange with a substantially smaller pool of bulk spins, determined by the detection limit of unbound 5F-BAPTA (~0.5 mM) as opposed to the nearly $10^5$-fold greater concentration of bulk water protons in the case of $^1$H CEST. While promising, CEST-based calcium sensors and $^{19}$F probes have been thus far restricted to *in vitro* imaging (to our knowledge) and critical challenges pertaining to sensitivity and imaging time need to be overcome before it becomes feasible to use these sensors in cellular and *in vivo* systems. In translating CEST to *in vivo* applications, care must also be taken to ensure minimum tissue heating from radio frequency deposition. While the general safety of CEST has been borne out by many studies in experimental vertebrates and humans, weaker or short-duration radio frequency pulses as well as alternative imaging sequences are available for CEST experiments requiring prolonged irradiation at high intensities that exceed specific absorption rate (SAR) limitations.

## VI. CONCLUSIONS AND OUTLOOK

MRI represents one of the most powerful techniques for simultaneous whole-brain imaging in any vertebrate species including non-human primates, which represent a valuable neuroscientific model for understanding complex behaviors and psychiatric diseases.[52,53] However, a central challenge with translating MRI-based calcium sensors into realistic *in vivo* paradigms relates to the limited sensitivity of contrast agents—the high concentrations of probes needed to produce statistically robust contrast being at odds with the low micromolar range of intracellular calcium fluctuations. While sensitivity can be improved through the use of superparamagnetic iron oxide nanoparticles, the larger size of these agents makes them harder to deliver to the vertebrate brain and coverage is limited to small volumes (e.g., 60 $\mu$L or ~12% of the rat brain[38]) Response kinetics of nanoparticle sensors also tend to be slower than small molecule probes. Another

limitation inherent to both small molecule and nanoparticle-based sensors is the inability to target them to genetically defined cell populations—a key shortcoming in light of the scientific breakthroughs enabled by the genetic precision of fluorescent calcium indicators such as GCaMP.[1–3] Genetic indicators also provide additional benefits unavailable with synthetic probes—for example, simplified *in vivo* delivery via viral vectors, suitability for repetitive long-term experiments, and compatibility with transgenic animals. To this end, several recent developments in biomolecular MRI have opened promising avenues for the development of genetically encoded calcium indicators. For instance, two newly developed classes of MRI reporters, based respectively on water channels (aquaporins) and gas-filled proteins (gas vesicles), offer improved sensitivity compared to earlier reporters, while also circumventing the need for paramagnetic metals.[54–56] Notably, fast-diffusing aquaporins (AQP) such as AQP1 have been found to elicit > 100% changes in diffusion-weighted MRI signals at 2–5 $\mu$M levels of protein expression.[55] Gas vesicles, while challenging to express genetically in mammalian cells, can be detected at picomolar concentrations by filling with $^{129}$Xe and using hyperpolarization techniques to enhance their spin polarization several-fold beyond Boltzmann distribution.[54] In the future, gas vesicles and/or aquaporins could serve as templates for building highly sensitive genetically encoded calcium indicators. Aside from the aforementioned all-genetic approaches, hybrid sensors could be developed by integrating current synthetic probe architectures with genetically expressed protein components—for example, by combining ester-protected $Gd^{3+}$ and $Mn^{3+}$-based calcium probes with cognate intracellularly encoded esterases. Paralleling these innovations in reporter gene technology are advances in neural gene delivery methods, including the use of focused ultrasound to transiently open the blood brain barrier and the development of viral serotypes that can enter the brain by crossing the blood brain barrier.[57,58] These technologies should eventually make it possible to deliver MRI reporters without surgery to spatially and genetically defined neurons, encompassing large brain volumes. Finally, it is worth noting that ongoing developments in MRI technology such as cryo-cooled probe heads, multi-slice imaging techniques, and faster sampling algorithms, will continue to push the boundaries of signal-to-noise and temporal resolution.[59,60] We anticipate that these advances will coincide with innovations in reporter gene technology, novel probe chemistries, and nanoparticle building blocks, thus establishing a rich toolset of calcium-responsive MRI sensors that eventually become a major driving force for fundamental breakthroughs in neuroscience and other areas of biology.

## AUTHORS' CONTRIBUTIONS

A.D.C.M. and H.F.O. are co-first authors and contributed equally to this work.

## ACKNOWLEDGMENTS

We thank members of the Mukherjee lab and our collaborators for helpful discussions. We thank Professor Mikhail Shapiro (Caltech) for insightful discussions on the topic of this review. Work related to this review has been supported by the California NanoSystems Institute (University of California, Santa Barbara), a NARSAD Young Investigator Award (to A.M.) from the Brain and Behavior Research Foundation, and a National Institutes of Health R35 Maximizing Investigators' Research Award (to A.M.).

## NOMENCLATURE

| | |
|---|---|
| MRI | magnetic resonance imaging |
| BAPTA | 1,2-bis(o-aminophenoxy)ethane-N,N,N′,N′-tetraacetic acid |
| APTRA | o-aminophenol-N,N,N-triacetic acid |
| EGTA | ethylene glycol-bis($\beta$-aminoethyl ether)-N,N,N′,N′-tetraacetic acid |
| CBP | calmodulin binding peptide |
| CEST | chemical exchange saturation transfer |
| AAZTA | 1,4-bis(carboxymethyl)-6-[bis(carboxymethyl)]-amino-6-methylperhydro-1,4-diazepine |
| AQP | aquaporins |

## APPENDIX A: BASIC PRINCIPLES OF $T_1$ AND $T_2$ CONTRAST

Inside an MRI scanner, the nuclear magnetic movement of water molecules (contained in cells and tissues) aligns with the external magnetic field, creating a longitudinal magnetization component. Spin–lattice relaxation describes the process by which this longitudinal magnetization returns to equilibrium after gaining energy from an on-resonance radio frequency pulse. Concurrently, this ensemble of excited nuclear spins also dephases from each other by a process known as spin–spin relaxation. These relaxation processes can be described by first order kinetics, which yields two time constants, $T_1$ and $T_2$, corresponding respectively to spin–lattice and spin–spin relaxation. When paramagnetic molecules or superparamagnetic crystals are introduced in a tissue, they shorten the $T_1$ and $T_2$ times of water protons, hence inducing a change in signal, which is detected as MRI contrast by applying specific image acquisition methods known as pulse sequences.

## APPENDIX B: CALCULATION OF $T_1$ CONTRAST FOR CALCIUM MRI SENSORS (TABLE I)

$T_1$ weighted signal intensity is computed from Eqs. (B1) and (B2).

$$\frac{S}{S_0} = \frac{\sin(\alpha)\left(1 - e^{-T_R \cdot R1}\right)}{1 - \cos(\alpha)e^{-T_R \cdot R1}} \tag{B1}$$

$$R_1 = R_{10} + \varphi(r_{1,on}.C_{bound}) + \varphi(r_{1,off}.C_{free}). \tag{B2}$$

| Parameter | Value |
|---|---|
| $R_{10}$ | 0.42 $s^{-1}$ |
| $\varphi$ (intracellular) | 0.80 |
| $\varphi$ (extracellular) | 0.20 |
| $T_R$ | 150 ms |
| $\alpha$ | 45 degrees |

Here, $\alpha$ is the flip angle; $T_R$ is repetition time; $R_1$ is relaxation rate (i.e., $1/T_1$) in the presence of the sensor; $R_{10}$ is background relaxation rate of brain tissue; $r_{1,on}$ and $r_{1,off}$ are relaxivities of the sensor

in calcium-bound and calcium-free states, respectively; $\varphi$ is the intracellular (extracellular) volume fraction for intracellular (extracellular) sensors; $C_{bound}$ and $C_{free}$ are sensor concentrations in calcium-bound and free states, respectively, calculated assuming equilibrium mass action kinetics and single-site binding with dissociation constants as reported in literature.

## DATA AVAILABILITY

Data sharing is not applicable to this review article as no new data were created or analyzed in this study. The data that supports the MRI signal intensity fold-change calculations depicted in Table I are available within the article (Appendix). Codes required to compute fold-changes are available from the corresponding author upon request.

## REFERENCES


[1]H. Dana, Y. Sun, B. Mohar, B. K. Hulse, A. M. Kerlin, J. P. Hasseman, G. Tsegaye, A. Tsang, A. Wong, and R. Patel, "High-performance calcium sensors for imaging activity in neuronal populations and microcompartments," Nat. Methods **16**(7), 649–657 (2019).

[2]Y. Zhao, S. Araki, J. Wu, T. Teramoto, Y.-F. Chang, M. Nakano, A. S. Abdelfattah, M. Fujiwara, T. Ishihara, and T. Nagai, "An expanded palette of genetically encoded $Ca^{2+}$ indicators," Science **333**(6051), 1888–1891 (2011).

[3]T.-W. Chen, T. J. Wardill, Y. Sun, S. R. Pulver, S. L. Renninger, A. Baohan, E. R. Schreiter, R. A. Kerr, M. B. Orger, and V. Jayaraman, "Ultrasensitive fluorescent proteins for imaging neuronal activity," Nature **499**(7458), 295–300 (2013).

[4]C. Grienberger and A. Konnerth, "Imaging calcium in neurons," Neuron **73**(5), 862–885 (2012).

[5]M. S. Rad, Y. Choi, L. B. Cohen, B. J. Baker, S. Zhong, D. A. Storace, and O. R. Braubach, "Voltage and calcium imaging of brain activity," Biophys. J. **113**(10), 2160–2167 (2017).

[6]A. Birkner, C. H. Tischbirek, and A. Konnerth, "Improved deep two-photon calcium imaging in vivo," Cell Calcium **64**, 29–35 (2017).

[7]A. Cheng, J. T. Gonçalves, P. Golshani, K. Arisaka, and C. Portera-Cailliau, "Simultaneous two-photon calcium imaging at different depths with spatio-temporal multiplexing," Nat. Methods **8**(2), 139–142 (2011).

[8]D. A. Dombeck, A. N. Khabbaz, F. Collman, T. L. Adelman, and D. W. Tank, "Imaging large-scale neural activity with cellular resolution in awake, mobile mice," Neuron **56**(1), 43–57 (2007).

[9]F. Helmchen and W. Denk, "Deep tissue two-photon microscopy," Nat. Methods **2**(12), 932–940 (2005).

[10]G. Hong, S. Diao, J. Chang, A. L. Antaris, C. Chen, B. Zhang, S. Zhao, D. N. Atochin, P. L. Huang, and K. I. Andreasson, "Through-skull fluorescence imaging of the brain in a new near-infrared window," Nat. Photonics **8**(9), 723–730 (2014).

[11]N. G. Horton, K. Wang, D. Kobat, C. G. Clark, F. W. Wise, C. B. Schaffer, and C. Xu, "In vivo three-photon microscopy of subcortical structures within an intact mouse brain," Nat. Photonics **7**(3), 205–209 (2013).

[12]J.-H. Park, W. Sun, and M. Cui, "High-resolution in vivo imaging of mouse brain through the intact skull," Proc. Nat. Acad. Sci. **112**(30), 9236–9241 (2015).

[13]K. T. Takasaki, D. Tsyboulski, and J. Waters, "Dual-plane 3-photon microscopy with remote focusing," Biomed. Opt. Express **10**(11), 5585–5599 (2019).

[14]K. Takasaki, R. Abbasi-Asl, and J. Waters, "Superficial bound of the depth limit of two-photon imaging in mouse brain," eNeuro **7**(1), ENEURO.0255–19.2019 (2020).

[15]G. Cui, S. B. Jun, X. Jin, M. D. Pham, S. S. Vogel, D. M. Lovinger, and R. M. Costa, "Concurrent activation of striatal direct and indirect pathways during action initiation," Nature **494**(7436), 238–242 (2013).

[16]K. K. Ghosh, L. D. Burns, E. D. Cocker, A. Nimmerjahn, Y. Ziv, A. E. Gamal, and M. J. Schnitzer, "Miniaturized integration of a fluorescence microscope," Nat. Methods **8**(10), 871 (2011).

[17]L. A. Gunaydin, L. Grosenick, J. C. Finkelstein, I. V. Kauvar, L. E. Fenno, A. Adhikari, S. Lammel, J. J. Mirzabekov, R. D. Airan, and K. A. Zalocusky, "Natural neural projection dynamics underlying social behavior," Cell **157**(7), 1535–1551 (2014).

[18]S. Ghosh, P. Harvey, J. C. Simon, and A. Jasanoff, "Probing the brain with molecular fMRI," Curr. Opin. Neurobiol. **50**, 201–210 (2018).

[19]T. Lee, L. X. Cai, V. S. Lelyveld, A. Hai, and A. Jasanoff, "Molecular-level functional magnetic resonance imaging of dopaminergic signaling," Science **344**(6183), 533–535 (2014).

[20]S. Ogawa, T.-M. Lee, A. R. Kay, and D. W. Tank, "Brain magnetic resonance imaging with contrast dependent on blood oxygenation," Proc. Nat. Acad. Sci. **87**(24), 9868–9872 (1990).

[21]X. Yu, Y. He, M. Wang, H. Merkle, S. J. Dodd, A. C. Silva, and A. P. Koretsky, "Sensory and optogenetically driven single-vessel fMRI," Nat. Methods **13**(4), 337–340 (2016).

[22]W.-h. Li, S. E. Fraser, and T. J. Meade, "A calcium-sensitive magnetic resonance imaging contrast agent," J. Am. Chem. Soc. **121**(6), 1413–1414 (1999).

[23]W.-h. Li, G. Parigi, M. Fragai, C. Luchinat, and T. J. Meade, "Mechanistic studies of a calcium-dependent MRI contrast agent," Inorg. Chem. **41**(15), 4018–4024 (2002).

[24]T. Atanasijevic, M. Shusteff, P. Fam, and A. Jasanoff, "Calcium-sensitive MRI contrast agents based on superparamagnetic iron oxide nanoparticles and calmodulin," Proc. Nat. Acad. Sci. **103**(40), 14707–14712 (2006).

[25]G. Angelovski, P. Fouskova, I. Mamedov, S. Canals, E. Toth, and N. K. Logothetis, "Smart magnetic resonance imaging agents that sense extracellular calcium fluctuations," ChemBioChem **9**(11), 1729–1734 (2008).

[26]K. Dhingra, P. Fousková, G. Angelovski, M. E. Maier, N. K. Logothetis, and E. Tóth, "Towards extracellular $Ca^{2+}$ sensing by MRI: Synthesis and calcium-dependent $^{1}H$ and $^{17}O$ relaxation studies of two novel bismacrocyclic $Gd^{3+}$ complexes," JBIC J. Biol. Inorg. Chem. **13**(1), 35–46 (2007).

[27]K. Dhingra, M. E. Maier, M. Beyerlein, G. Angelovski, and N. K. Logothetis, "Synthesis and characterization of a smart contrast agent sensitive to calcium," Chem. Commun. **29**, 3444–3446 (2008).

[28]V. Kubíček, T. Vitha, J. Kotek, P. Hermann, L. Vander Elst, R. N. Muller, I. Lukeš, and J. A. Peters, "Towards MRI contrast agents responsive to Ca(II) and Mg(II) ions: Metal-induced oligomerization of dota–bisphosphonate conjugates," Contrast Media Mol. Imag. **5**(5), 294–296 (2010).

[29]I. Mamedov, S. Canals, J. Henig, M. Beyerlein, Y. Murayama, H. A. Mayer, N. K. Logothetis, and G. Angelovski, "In vivo characterization of a smart MRI agent that displays an inverse response to calcium concentration," ACS Chem. Neurosci. **1**(12), 819–828 (2010).

[30]G. Angelovski, T. Chauvin, R. Pohmann, N. K. Logothetis, and É. Tóth, "Calcium-responsive paramagnetic CEST agents," Bioorganic Medic. Chem. **19**(3), 1097–1105 (2011).

[31]A. Bar-Shir, A. A. Gilad, K. W. Y. Chan, G. Liu, P. C. M. van Zijl, J. W. M. Bulte, and M. T. McMahon, "Metal ion sensing using ion chemical exchange saturation transfer $^{19}F$ magnetic resonance imaging," J. Am. Chem. Soc. **135**(33), 12164–12167 (2013).

[32]G. Angelovski, S. Gottschalk, M. Milošević, J. Engelmann, G. E. Hagberg, P. Kadjane, P. Andjus, and N. K. Logothetis, "Investigation of a calcium-responsive contrast agent in cellular model systems: Feasibility for use as a smart molecular probe in functional MRI," ACS Chem. Neurosci. **5**(5), 360–369 (2014).

[33]P. Kadjane, C. Platas-Iglesias, P. Boehm-Sturm, V. Truffault, G. E. Hagberg, M. Hoehn, N. K. Logothetis, and G. Angelovski, "Dual-frequency calcium-responsive MRI agents," Chem. – A Eur. J. **20**(24), 7351–7362 (2014).

[34]S. Gündüz, N. Nitta, S. Vibhute, S. Shibata, M. E. Mayer, N. K. Logothetis, I. Aoki, and G. Angelovski, "Dendrimeric calcium-responsive MRI contrast agents with slow in vivo diffusion," Chem. Commun. **51**(14), 2782–2785 (2015).

[35]A. Moussaron, S. Vibhute, A. Bianchi, S. Gündüz, S. Kotb, L. Sancey, V. Motto-Ros, S. Rizzitelli, Y. Crémillieux, and F. Lux, "Ultrasmall nanoplatforms as calcium-responsive contrast agents for magnetic resonance imaging," Small **11**(37), 4900–4909 (2015).

[36]K. W. MacRenaris, Z. Ma, R. L. Krueger, C. E. Carney, and T. J. Meade, "Cell-permeable esterase-activated Ca(II)-sensitive MRI contrast agent," Bioconjugate Chem. **27**(2), 465–473 (2016).

[37]A. T. Preslar, L. M. Lilley, K. Sato, S. Zhang, Z. K. Chia, S. I. Stupp, and T. J. Meade, "Calcium-induced morphological transitions in peptide amphiphiles detected by $^{19}$F-magnetic resonance imaging," ACS Appl. Mater. Interfaces **9**(46), 39890–39894 (2017).
[38]S. Okada, B. B. Bartelle, N. Li, V. Breton-Provencher, J. J. Lee, E. Rodriguez, J. Melican, M. Sur, and A. Jasanoff, "Calcium-dependent molecular fMRI using a magnetic nanosensor," Nat. Nanotechnol. **13**(6), 473–477 (2018).
[39]A. Barandov, B. B. Bartelle, C. G. Williamson, E. S. Loucks, S. J. Lippard, and A. Jasanoff, "Sensing intracellular calcium ions using a manganese-based MRI contrast agent," Nat. Commun. **10**(1), 897 (2019).
[40]K. Du, A. E. Thorarinsdottir, and T. D. Harris, "Selective binding and quantitation of calcium with a cobalt-based magnetic resonance probe," J. Am. Chem. Soc. **141**(17), 7163–7172 (2019).
[41]T. Savić, G. Gambino, V. S. Bokharaie, H. R. Noori, N. K. Logothetis, and G. Angelovski, "Early detection and monitoring of cerebral ischemia using calcium-responsive MRI probes," Proc. Nat. Acad. Sci. **116**(41), 20666–20671 (2019).
[42]C. J. Adams, R. Krueger, and T. J. Meade, "A multimodal Ca(II) responsive near IR-MR contrast agent exhibiting high cellular uptake," ACS Chem. Biol. **15**(2), 334–341 (2020).
[43]G. Gambino, T. Gambino, R. Pohmann, and G. Angelovski, "A ratiometric $^{19}$F MR-based method for the quantification of $Ca^{2+}$ using responsive paramagnetic probes," Chem. Commun. **56**(24), 3492–3495 (2020).
[44]F. Garello, S. Gündüz, S. Vibhute, G. Angelovski, and E. Terreno, "Dendrimeric calcium-sensitive MRI probes: The first low-field relaxometric study," J. Mater. Chem. B **8**(5), 969–979 (2020).
[45]A. Bar-Shir, L. Avram, S. Yariv-Shoushan, D. Anaby, S. Cohen, N. Segev-Amzaleg, D. Frenkel, O. Sadan, D. Offen, and Y. Cohen, "Alginate-coated magnetic nanoparticles for noninvasive MRI of extracellular calcium," NMR Biomedicine **27**(7), 774–783 (2014).
[46]U. Heinemann, H. Lux, and M. Gutnick, "Extracellular free calcium and potassium during paroxysmal activity in the cerebral cortex of the cat," Exp. Brain Res. **27**(3–4), 237–243 (1977).
[47]C. Nicholson, G. T. Bruggencate, R. Steinberg, and H. Stöckle, "Calcium modulation in brain extracellular microenvironment demonstrated with ion-selective micropipette," Proc. Nat. Acad. Sci. **74**(3), 1287–1290 (1977).
[48]G. E. Hagberg, I. Mamedov, A. Power, M. Beyerlein, H. Merkle, V. G. Kiselev, K. Dhingra, V. Kubìček, G. Angelovski, and N. K. Logothetis, "Diffusion properties of conventional and calcium-sensitive MRI contrast agents in the rat cerebral cortex," Contrast Media Mol. Imag. **9**(1), 71–82 (2014).
[49]F. Garello, S. Vibhute, S. Gündüz, N. K. Logothetis, E. Terreno, and G. Angelovski, "Innovative design of Ca-sensitive paramagnetic liposomes results in an unprecedented increase in longitudinal relaxivity," Biomacromolecules **17**(4), 1303–1311 (2016).
[50]J. M. Perez, L. Josephson, T. O'Loughlin, D. Högemann, and R. Weissleder, "Magnetic relaxation switches capable of sensing molecular interactions," Nat. Biotechnol. **20**(8), 816–820 (2002).
[51]P. C. Van Zijl and N. N. Yadav, "Chemical exchange saturation transfer (CEST): What is in a name and what isn't?," Magn. Resonance Medicine **65**(4), 927–948 (2011).
[52]K. K. Watson and M. L. Platt, "Of mice and monkeys: Using non-human primate models to bridge mouse-and human-based investigations of autism spectrum disorders," J. Neurodevelopmental Disorders **4**(1), 21 (2012).
[53]A. S. Mitchell, A. Thiele, C. I. Petkov, A. Roberts, T. W. Robbins, W. Schultz, and R. Lemon, "Continued need for non-human primate neuroscience research," Curr. Biol. **28**(20), PR1186 (2018).
[54]M. G. Shapiro, R. M. Ramirez, L. J. Sperling, G. Sun, J. Sun, A. Pines, D. V. Schaffer, and V. S. Bajaj, "Genetically encoded reporters for hyperpolarized xenon magnetic resonance imaging," Nat. Chem. **6**(7), 629–634 (2014).
[55]A. Mukherjee, D. Wu, H. C. Davis, and M. G. Shapiro, "Non-invasive imaging using reporter genes altering cellular water permeability," Nat. Commun. **7**, 13891 (2016).
[56]A. Mukherjee, H. C. Davis, P. Ramesh, G. J. Lu, and M. G. Shapiro, "Biomolecular MRI reporters: Evolution of new mechanisms," Prog. Nuclear Magnetic Resonance Spectroscopy **102–103**, 32–42 (2017).
[57]K. Y. Chan, M. J. Jang, B. B. Yoo, A. Greenbaum, N. Ravi, W.-L. Wu, L. Sánchez-Guardado, C. Lois, S. K. Mazmanian, and B. E. Deverman, "Engineered AAVs for efficient noninvasive gene delivery to the central and peripheral nervous systems," Nat. Neurosci. **20**(8), 1172–1179 (2017).
[58]J. O. Szablowski, A. Lee-Gosselin, B. Lue, D. Malounda, and M. G. Shapiro, "Acoustically targeted chemogenetics for the non-invasive control of neural circuits," Nat. Biomed. Eng. **2**(7), 475 (2018).
[59]M. Barth, F. Breuer, P. J. Koopmans, D. G. Norris, and B. A. Poser, "Simultaneous multislice (SMS) imaging techniques," Magn. Resonance Medicine **75**(1), 63–81 (2016).
[60]J. C. Ye, "Compressed sensing MRI: A review from signal processing perspective," BMC Biomed. Eng. **1**(1), 8 (2019).